ChemPubSoc Europe

DOI: 10.1002/chem.201600652

CHEMISTRY A European Journal Full Paper

Organic Semiconductors

Modulation of the Physicochemical Properties of Donor–Spiro–Acceptor Derivatives through Donor Unit Planarisation: Phenylacridine versus Indoloacridine. New Hosts for Green and Blue Phosphorescent Organic Light-Emitting Diodes (PhOLEDs)

Sébastien Thiery,[a] Denis Tondelier,[c] Bernard Geffroy,[b, c] Olivier Jeannin,[a] Joëlle Rault-Berthelot,*[a] and Cyril Poriel*[a]

Abstract: This work reports a detailed structure–property relationship study of a series of efficient host materials based on the donor–spiro–acceptor (D-spiro-A) design for green and sky-blue phosphorescent organic light-emitting diodes (PhOLEDs). The electronic and physical effects of the indoloacridine (IA) fragment connected through a spiro bridge to different acceptor units, namely, fluorene, dioxothioxanthene or diazafluorene moiety, have been investigated in depth. The resulting host materials have been easily synthesised through short, efficient, low-cost, and highly adaptable synthetic routes by using common intermediates. The dyes possess a very high triplet energy (E_T) and tuneable HOMO/LUMO levels, depending on the strength of the donor/acceptor combination. The peculiar electrochemical and optical properties of the IA moiety have been investigated though a fine comparison with their phenylacridine counterparts to study the influence of planarisation. Finally, these molecules have been incorporated as hosts in green and sky-blue PhOLEDs. For the derivative SIA-TXO_2 as a host, external quantum efficiencies as high as 23 and 14% have been obtained for green and sky-blue PhOLEDs, respectively.

Introduction

The achievement of efficient and stable organic light-emitting diodes (OLEDs)[1] and/or phosphorescent organic light-emitting diodes (PhOLEDs),[2] in view of obtaining new, low-cost displays and lightings, has been the research field of many chemists and physicists in the last 30 years. In an OLED, the organic emitting layer (EML) emits light from singlet excitons formed under the effect of the powering up of the device and due to the singlet/triplet excitons ratio of 25/75, the internal quantum efficiency (IQE) of an OLED is limited to 25% (the triplet excitons are lost in non-radiative deactivation processes).[1a,c] In a PhOLED, the EML is constituted of an organic host doped with a phosphorescent metal complex, which allows the use of both singlet and triplet excitons in the emission process,[2c] leading to a possible IQE of 100%.[3] The development of numerous organic materials as hosts in PhOLEDs has led to highly efficient red,[4] yellow,[5] and green[6] phosphorescent devices, whereas blue devices, despite fantastic recent progress, remain the weak link of this technology.[2a,c–e,7] Indeed, the necessary requirements for the host are manifold: 1) a high thermal stability (to avoid the decomposition of the material during operation of the device); 2) the adequacy of the HOMO–LUMO energy levels to Fermi levels of the electrodes to facilitate charge injection into the EML; 3) equilibrated electron and hole mobilities to guarantee efficient electron/hole recombination in the host; and 4) a triplet energy, E_T, of the host higher than that of the dopant to allow host–guest exciton transfer, while avoiding reverse guest–host exciton transfer. Combining all of these properties in a single host is not an easy task for blue emission and is the subject of intense academic research. Indeed, the E_T of blue phosphors is higher than 2.6 eV (E_T FIrpic[8] = 2.62 eV (FIrpic = bis[2-(4,6-difluorophenyl)pyridinato-C^2,*N*](picolinato)iridium(III)), E_T FIrtaz[9] = 2.69 eV (FIrtaz = bis(4,6-difluorophenylpyridinato)[5-(pyridine-2-yl)-1,2,4-triazolato]iridium(III)), E_T FIrN4[9] = 2.70 eV (FIrN4 = bis(4,6-difluorophenylpyridinato)[5-(pyridin-2-yl)tetrazolato]iridium(III)), or even for the bluest emitting dopants, E_T FCNIr = 2.8 eV[10] (FCNIr = bis[(3,5-difluoro-4-cyanophenyl)pyridine]iridium(III)) or E_T [Ir(dfpypy)$_3$][11] (dfpypy = 2′,6′-difluoro-2,3′-bipyridinato-N,$C^{4'}$) and E_T FK306[12] = 2.83 eV (FK306, bis(4-*tert*-butyl-2′,6′-difluoro-2,3′-bipyridine)(acetylacetonate)iridium(III))), and hence, the E_T

[a] Dr. S. Thiery, Dr. O. Jeannin, Dr. J. Rault-Berthelot, Dr. C. Poriel
UMR CNRS 6226 "Institut des Sciences Chimiques de Rennes"
Université de Rennes 1-Campus de Beaulieu
35042 Rennes Cedex (France)
E-mail: Joelle.Rault-Berthelot@univ-rennes1.fr
cyril.poriel@univ-rennes1.fr

[b] B. Geffroy
LICSEN, NIMBE, CEA, CNRS, Université Paris-Saclay
CEA Saclay 91191 Gif Sur Yvette (France)

[c] Dr. D. Tondelier, B. Geffroy
LPCIM, CNRS, École Polytechnique, Université Paris-Saclay
91128 Palaiseau (France)

Supporting information for this article is available on the WWW under http://dx.doi.org/10.1002/chem.201600652.

of an efficient host for blue phosphorescent emission should be at least 2.7 eV.

To guarantee a high E_T, wide energy gap materials are usually designed.[7b,c,13] However, due to the deep HOMO and high LUMO levels of wide band gap materials, simultaneously injecting holes and electrons into the host is difficult and requires multilayer devices, leading to high costs and a high turn-on voltage (V_{on}). One solution is to design bipolar molecules,[2d,e,14] in which the donor and acceptor units are on two non-conjugated π systems; this avoids a decrease in the singlet and triplet energies required for blue emission. Recently, our groups designed new, efficient host materials for green and blue PhOLEDs by using a new molecular design called donor–spiro–acceptor (D-spiro-A)[15] based on the connection of a donor unit and an acceptor unit through an insulating spiro bridge.[7c,16] Among them, two semiconductors, **SPA-DAF** and **SPA-TXO$_2$** (Scheme 1), in which the donor phenylacridine (PA) unit is linked through a spiro carbon to the diazafluorene (DAF) or dioxothioxanthene (TXO_2) acceptor units. **SPA-DAF** and **SPA-TXO$_2$** have electrochemical gaps of 3.04 and 3.43 eV, respectively, and very high E_T values of 2.98 and 3.08 eV, respectively. These two compounds have been used as hosts for FIrpic, leading to efficient devices.[16]

There are few reports in the literature of examples of materials possessing fused N-phenylcarbazole, also named indoloacridine (IA). In a first class, the IA core is di-substituted at the methylene position (see IA core in blue in Scheme 2); in a second class, the IA core is connected to a fluorene (F) through a spiro carbon (see the spiro–IA–F (SIAF) core in red in Scheme 2).[17] Except for **ACDCN** (Scheme 2, bottom), which possesses an energy gap of 2.68 eV, due to substitution in positions 2 and 7 of the F unit, which extends the π conjugation, all IA or SIAF derivatives presented in Scheme 2 possess a large energy gap (close to 3.4 eV) and E_T values in the range of 2.72–2.95 eV, leading to their use as host materials for blue phosphors. In some cases, the resulting PhOLEDs displayed high performance.

However, the properties of the IA fragment remain relatively unknown. Thus, to precisely study the influence of stiffening of the donor group (IA versus PA) and to obtain high-per-

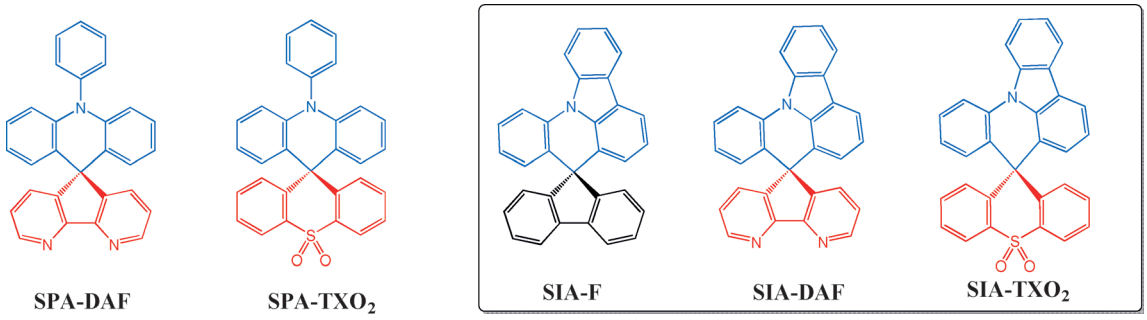

Scheme 1. Structure of some D-spiro-A molecules;[16] the target molecules of this work are highlighted in the box.

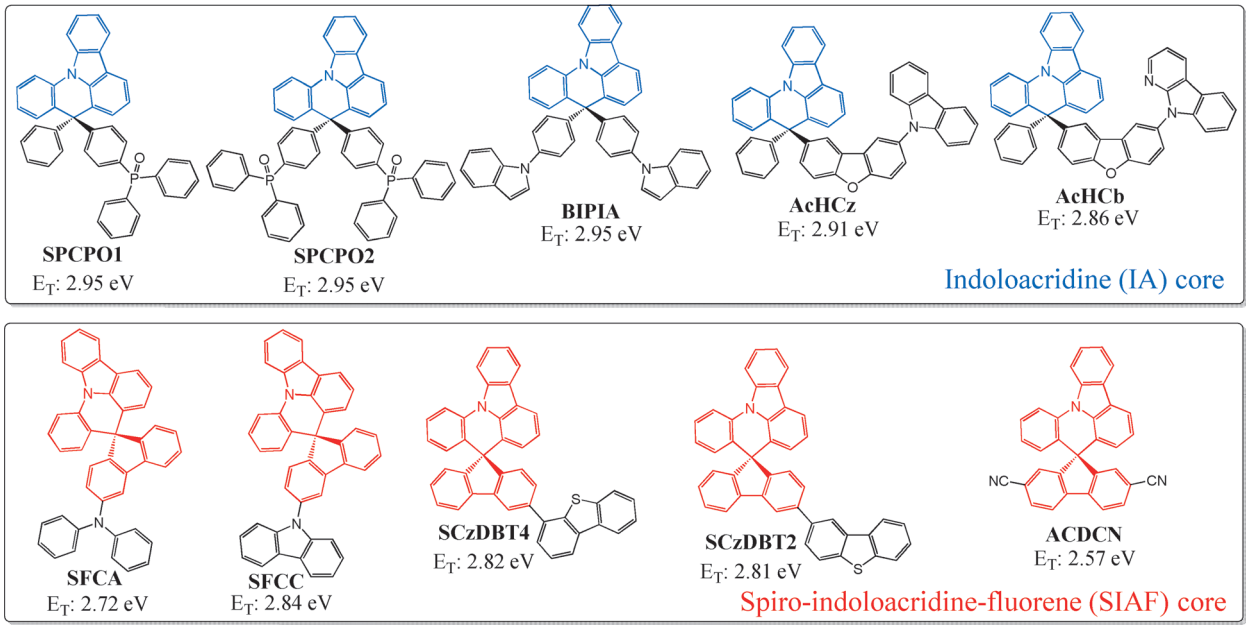

Scheme 2. Indoloacridine- (IA) and spiroindoloacridine (SIA)-type host materials reported in the literature.[17]

formance blue PhOLEDs, we decided to investigate new D-spiro-A molecules composed of an IA core as a donor unit connected to either DAF or TXO_2 cores as the acceptor unit.

Hence, compounds **SIA-DAF** and **SIA-TXO_2** were synthesised, and their physicochemical/photophysical properties and device performances were studied in depth and compared with those of structurally related model compound **SIA-F**, which possessed a F fragment as the acceptor unit (see the structures of the three molecules in Scheme 1). This will allow to define a precise structure/properties relationship for IA based organic semi-conductors, key feature for the future of this donor group in organic electronics.

Results and Discussion

Synthesis

An important feature for the future mass production of host materials is to set up highly efficient and short synthetic approaches. Ideally, the route should allow various host materials to be obtained from common intermediates. The synthesis of **SIA-DAF**, **SIA-TXO_2** and **SIA-F** starts with the synthesis of 9-(2-bromophenyl)-*9H*-carbazole (**1**), which is obtained through the copper-catalysed C–N bond coupling of 1,2-dibromobenzene and carbazole in 58% yield (Scheme 3).[18] Lithium–halogen exchange between **1** and *n*BuLi, followed by trapping of the lithiated intermediate with the corresponding ketone (9*H*-fluorenone, 9*H*-4,5-diazafluorenone[16b,19] or 9*H*-10,10-dioxothioxanthenone[16]), provides the corresponding tertiary alcohol (not isolated). An intramolecular electrophilic cyclisation in strong acidic media (MsOH) finally provides **SIA-F**, **SIA-DAF** and **SIA-TXO_2** in relatively good yields (52, 41 and 44%, respectively, over two steps). Thus, from the common intermediate **1**, three SIA-based semiconductors incorporating different acceptor units have been readily and efficiently obtained; this highlights the efficiency of the present approach. In addition, it should be stressed that the present synthetic approach does not involve any palladium catalysts and is therefore a low-cost route, which is a key feature for the future of OLED technology.

Structural properties

The molecular structures of **SIA-F** and **SIA-TXO_2** (no single crystals were obtained for **SIA-DAF**) have been confirmed by X-ray crystallography on single crystals (slow evaporation of solutions of dichloromethane or dichloromethane/methanol). X-ray data for both compounds reveal an asymmetric unit containing four independent molecules for **SIA-F** and only one molecule for **SIA-TXO_2** (Figure 1 and Table 1; more details are provided in Figures S1–S25 in the Supporting Information).

The molecular radius of each molecule (distance from the spiro carbon atom to the farthest carbon atom (orange arrow in Figure 1)) has been evaluated between 6.95 and 7.02 Å for **SIA-F**s and 7.00 Å for **SIA-TXO_2**. Thus, the radius of **SIA-TXO_2** is slightly shorter than that of previously reported **SPA-TXO_2** (7.14 Å)[16b] due to the structural difference between the PA and IA units. The slight variation of the **SIA-F** radii in the four different molecules present in the asymmetric unit is due to modulation of the planarity of the IA core. Indeed, in **SIA-TXO_2**, the IA core appears to be nearly planar (angle between the mean planes of rings 1 and 5 of 5.37°), whereas in **SIA-F**

Table 1. Main structural characteristics of **SIA-F** (*Mol1–Mol4*) and of **SIA-TXO_2**.

	SIA-F				SIA-TXO_2
	Mol1	*Mol2*	*Mol3*	*Mol4*	
F or TXO_2 deformation angle[a] [°]	3.04	3.28	1.13	4.65	13.00
IA deformation angle[b] [°]	15.46	4.22	19.46	8.26	5.37
Acridine deformation angle[c] [°]	14.73	3.20	15.91	7.27	2.90
Carbazole deformation angle[d] [°]	1.40	1.15	3.73	3.26	2.84
Spiro angle[e] [°]	88.69	87.98	89.77	89.03	87.12
Radius[f] [Å]	6.95	7.02	6.98	7.02	7.00

[a] Angle between mean planes of the two external phenyl rings (6 and 8). [b] Angle between mean planes of rings 1 and 5. [c] Angle between mean planes of rings 3 and 5. [d] Angle between mean planes of rings 1 and 3. [e] Angle between the mean plane of rings 4 and 7. [f] Distance from the spiro carbon atom to the farthest carbon atom.

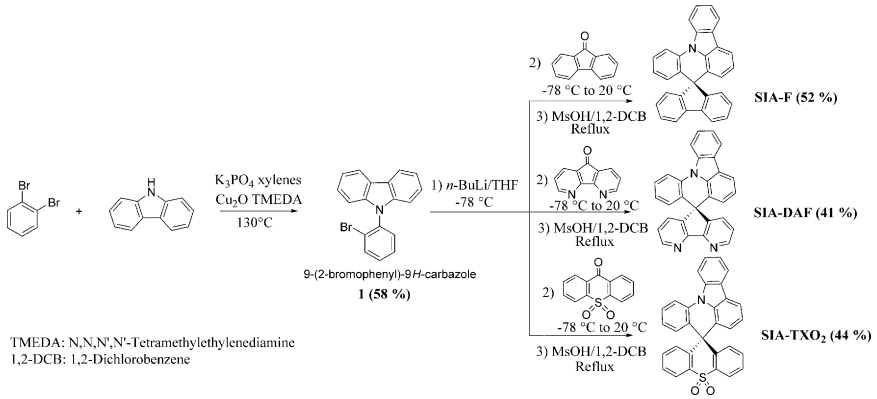

Scheme 3. Syntheses of **SIA-F**, **SIA-DAF** and **SIA-TXO_2**. TMEDA = *N*,*N*,*N*′,*N*′-tetramethylethylenediamine, MsOH = methanesulfonic acid, 1,2-DCB = 1,2-dichlorobenzene.

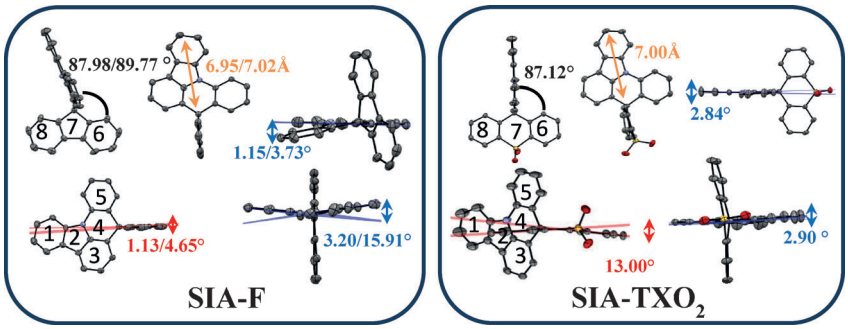

Figure 1. Molecular structures obtained by X-ray crystallography. Left: **SIA-F** (exemplified by *Mol3* with extreme values of different parameters in the four **SIA-Fs** molecules, *Mol1* to *Mol4*; see Table 1 for values of each molecule); right: **SIA-TXO$_2$**. Hydrogen atoms have been omitted for clarity. Ellipsoids are drawn at the 50% probability level.[29]

the corresponding dihedral angles vary from 4.22 to 19.46°; this shows a clear distortion of the IA core in **SIA-F** *Mol1* and *Mol3*. The higher rigidity of the F core (F deformation between 1.13 and 4.65°; Table 1) compared with that of **TXO$_2$** (13.0°) induces a stronger deformation of the acridine core in **SIA-F** than that found in **SIA-TXO$_2$** (acridine deformation is measured to be from 3.20 to 15.91° in **SIA-Fs** and at 2.90° in **SIA-TXO$_2$**), and therefore, a stronger deformation of the IA cores. In D-spiro-A molecules, this highlights the strong impact of the acceptor unit (F versus TXO$_2$) on the deformation of the rigid IA core. Similar deformations as a function of the acceptor unit have been previously observed for other D-spiro-A molecules possessing the PA core, and hence, this seems to be a general feature of such structures.[16b] One can note that the deformation of the IA cores is mainly governed by acridine deformation because carbazole deformation, measured by the angle between rings 1 and 3, remains weak in both **SIA-F** (carbazole deformation between 1.15 and 3.73°) and **SIA-TXO$_2$** (carbazole deformation 2.84°).

In all molecules, the donor and acceptor fragments are almost orthogonal with a twist angle between the mean plane of rings 4 and 7 of 87.12° in **SIA-TXO$_2$** and around 88.9° in **SIA-F** (88.69, 87.98, 89.77, and 89.03° in *Mol1*, *Mol2*, *Mol3*, and *Mol4*, respectively). Notably, in **SIA-F** *Mol1* and *Mol3*, the important deformation of the IA units (15.46 and 19.46° in *Mol1* and *Mol3*, respectively; see Table 1) renders the calculation of the mean plane of the ring 4 more difficult, and therefore, leads to less precise information.

Thermal properties

The thermal properties of the three compounds were investigated by thermogravimetric analysis (TGA) and differential scanning calorimetry (DSC). Indeed, good thermal stability is needed before any possible OLED applications.

Because a total mass loss is observed, without any intermediate decomposition step, we believe that complete mass loss may be attributed to a sublimation process of the molecules at temperatures higher than 320 °C. Very high stability was also observed for the PA analogues, with a total mass loss measured at more than 350 °C for **SPA-DAF** and **SPA-TXO$_2$**.[16b]

DSC studies (see Figures S27, S29, and S31 in the Supporting Information) do not reveal phase transitions for **SIA-DAF** or **SIA-TXO$_2$**; only one glass transition, T_g, is observed for **SIA-F** at 94 °C. This T_g value is slightly higher than that of 9,9′-spirobifluorene (**9,9′-SBF**: T_g = 80 °C),[13a] which indicates that the replacement of an F fragment by an IA core increases the value of T_g. This T_g value is also higher than that of classical host materials for PhOLEDs, such as *N*,*N*′-dicarbazolyl-4,4′-biphenyl (CBP; T_g = 62 °C)[20] or 1,3-bis(9-carbazolyl)benzenz (*m*-CP; T_g = 55 °C).[9] No recrystallisation transition occurs for the three compounds.

Electrochemical properties

The electrochemical properties have been investigated by cyclic voltammetry (CV) in CH_2Cl_2 for oxidation and reduction (Figure 2 and Table 2; potentials are given versus a saturated calomel electrode (SCE)). In the reduction process, compounds **SIA-F** and **SIA-TXO$_2$** do not present any reduction waves before −3.25 V, whereas **SIA-DAF** presents an irreversible reduction with a maximum at −2.49 V (Figure 2 A, red line). From their onset reduction potentials measured at −2.52, −2.13 and −2.35 V, we determined LUMO energies of −1.88 eV for **SIA-F**, −2.27 eV for **SIA-DAF** and −2.05 eV for **SIA-TXO$_2$**. Because the donor fragment is identical for the three compounds, we can precisely classify the strength of the acceptor unit as follows: DAF > TXO$_2$ > F. The +0.22 eV shift of the LUMO level from **SIA-DAF** to **SIA-TXO$_2$** is in accordance with the +0.31 eV shift previously observed in the SPA series (LUMO: −2.31 eV for **SPA-DAF** and −2 eV for **SPA-TXO$_2$**).[16b] Because the LUMO energy levels of **SIA-DAF** and **SIA-TXO$_2$** are slightly different from those of their PA counterparts, namely, **SPA-DAF** and **SPA-TXO$_2$**, the donor may also have an influence on acceptor reduction through the spiro bridge.

In oxidation, compound **SIA-F** presents two successive oxidation processes with peak potentials at E^1 = 1.19 V and E^2 ≈ 1.80 V (Figure 2 B, black line). Regardless of the sweep rate, the first oxidation remains irreversible, which shows the high reactivity of the radical cation formed in this first oxidation process. Recurrent sweeps, including the two oxidation waves, lead to electropolymerisation processes (see Figure S47 in the Supporting Information) classically observed for F deriva-

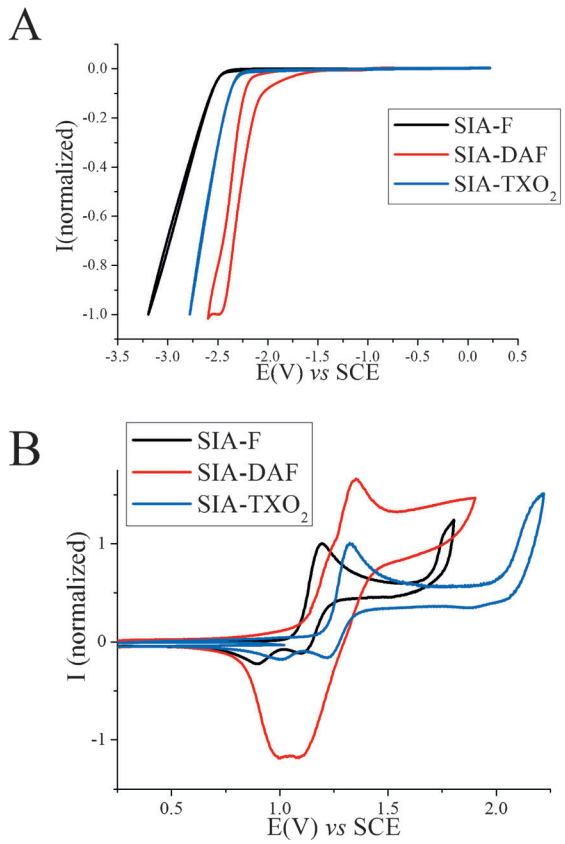

Figure 2. Cyclic voltammograms of **SIA-F**, **SIA-DAF** and **SIA-TXO$_2$**, in the cathodic (A) or the anodic (B) range, recorded in $CH_2Cl_2 + Bu_4NPF_6$ (0.2 M) at a sweep rate of 100 mV s^{-1}. Platinum disk (diameter 1 mm) working electrode. The cyclic voltammograms are normalised in current towards their first reduction (A) or oxidation (B) processes.

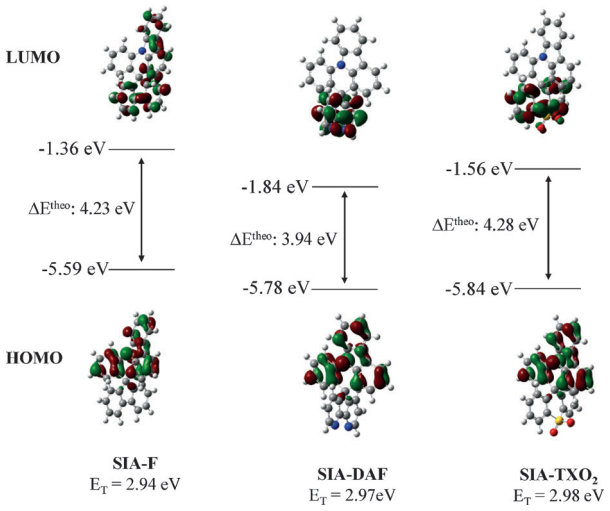

Figure 3. Frontier molecular orbitals calculated by DFT of **SIA-F**, **SIA-DAF** and **SIA-TXO$_2$**, after geometry optimisation at the B3LYP/6-311G + (d,p) level of theory, shown with an isovalue of 0.04.

Table 2. Electronic properties obtained by theoretical calculations, electrochemical studies and optical studies of **SIA-F**, **SIA-DAF** and **SIA-TXO$_2$**.

	Theoretical calculations				Electrochemical data			Optical data	
	LUMO[a]	HOMO[a]	ΔE^{theo}[a]	E_T^{theo}[a]	LUMO[b]	HOMO[b]	ΔE^{el}[b]	ΔE^{opt}[c]	E_T^{opt}[d]
SIA-F	−1.36	−5.59	4.23	2.94	−1.88	−5.48	3.60	3.41	2.87
SIA-DAF	−1.84	−5.78	3.94	2.97	−2.27	−5.50	3.23	3.42	2.89
SIA-TXO$_2$	−1.56	−5.84	4.28	2.98	−2.05	−5.61	3.56	3.42	2.93

[a] Obtained from theoretical calculations on the optimisation geometry. [b] Obtained from electrochemical analyses. [c] Obtained from absorption spectra in cyclohexane. [d] Obtained from low-temperature (77 K) emission spectra.

tives.[21] Compared with **9,9′-SBF**, the oxidation of which occurs at 1.68 and 1.88 V,[13a,21b,22] the first oxidation of **SIA-F** occurs at a 0.49 V less anodic potential. This leads us to conclude that the first oxidation involves the IA core, whereas the second oxidation involves the F unit. The assignment of the first electron transfer on the IA core of **SIA-F** is also supported by HOMO localisation (Figure 3) and the calculated spin density of the cation radical of **SIA-F**, which is mainly centred on the IA part of **SIA-F** (Figure S55 in the Supporting Information).

Compound **SIA-DAF** (Figure 2B, red line) presents two very close successive reversible oxidation processes between 1.0 and 1.5 V (the wave with a maximum at 1.34 V is clearly preceded by a shoulder even more clearly shown through CV recorded up to 1.5 V and through differential pulse voltammetry (DPV); Figure S48 in the Supporting Information). No polymerisation process was observed for **SIA-DAF**.

Finally, compound **SIA-TXO$_2$** (Figure 2B, blue line) presents two successive oxidation waves at potentials more anodic than 1.2 V. The first irreversible wave is centred at 1.33 V, whereas the second is centred at about 2.2 V. Recording successive cycles in the potential range, including the two oxidation waves, show only a weak polymerisation process (Figure S49 in the Supporting Information).

Because the first electron transfer is assigned for the three compounds to the IA core, the different first oxidation potentials observed clearly indicate the influence of the acceptor unit on the donor oxidation. This is a significant feature in the tuning of the HOMO levels.

From the onset of their first oxidation waves measured at 1.08, 1.10 and 1.21 V, we determined the HOMO levels of the three compounds at −5.48 eV for **SIA-F**, −5.50 eV for **SIA-DAF** and −5.61 eV for **SIA-TXO$_2$**. These HOMO levels are 1) all higher than that of **9,9′-SBF** (−5.94 eV),[13a] as a result of the stronger donor character of IA versus F, and 2) all lower than those of **SPA-DAF** and **SPA-TXO$_2$** (−5.35 and −5.42 eV, respectively).[16b] Thus, the weak shift of 0.11 eV between the HOMO of **SIA-DAF** and that of **SIA-TXO$_2$** is in accordance with the shift of 0.07 eV recorded between the HOMOs of **SPA-DAF** and **SPA-TXO$_2$**; this shows the similar effect of the acceptor units DAF or TXO_2 on the donor units (PA versus IA). This trend is nevertheless surprising because DAF is a stronger acceptor unit than TXO_2, and hence, DAF should theoretically decrease the HOMO level more than TXO_2.

Because the opposite trend is observed for both IA and PA series (and also predicted by theoretical calculations, see below), structural features (different distortions and planarity of the IA/PA core) and/or unusual electronic influence of the spiro carbon may be involved. These unusual features deserve to be unravelled in the future for D-spiro-A compounds.

Another important feature deserves to be stressed. The HOMO levels of the SIA series are deeper than those of the SPA series by around 0.15–0.19 eV; this seems to be very surprising and uncommon. Indeed, greater planarity of the structure, which increases π conjugation (such as in SIA versus SPA), results in a higher HOMO level. Similar decreases in the HOMO levels have been reported by other groups, when comparing the HOMO of IA compounds with those of their PA counterparts.[23,17e,24] Such a lowering of the HOMO levels is also observed in theoretical calculations of 1) *N*-phenylcarbazole/indolocarbazole (HOMO: −5.69/−5.91 eV) versus PA/IA (HOMO: −5.29/−5.55 eV; see related theoretical calculations in Figures S50 and S51 in in the Supporting Information), and 2) **SPA-DAF**/**SPA-TXO$_2$** (−5.49/−5.57 eV)[16b] versus **SIA-DAF**/**SIA-TXO$_2$** (−5.78/−5.84 eV; Figure 3). Thus, the decrease in the HOMO level of IA versus the PA core was assigned by Jiang et al. to the energy levels of the constituting blocks.[17e] Indeed, the significant difference in LUMO energy levels between the biphenyl (found in IA) and phenyl (found in PA) units is invoked by the authors to explain the decrease in the HOMO level of IA versus that of PA. This decrease in the HOMO levels through stiffening of the PA core appears to be a general and important feature of the SIA derivatives.

From the HOMO and LUMO levels, we calculated the electrochemical gap, ΔE^{el}, of the three compounds at 3.60 eV for **SIA-F**, 3.23 eV for **SIA-DAF** and 3.56 eV for **SIA-TXO$_2$**. These ΔE^{el} values are wider than those of the PA analogues **SPA-DAF** (3.04 eV) and **SPA-TXO$_2$** (3.43 eV),[16b] mainly due to the higher HOMO levels of PA compounds. Thus, the ΔE^{el} values of **SIA-DAF** and **SIA-TXO$_2$** are different and reflect the different strengths of the acceptor fragments (very different LUMO energy levels) and different electronic and/or structural effects on the oxidation of the IA core (slightly different HOMO energy levels).

Geometry optimisation of the three compounds was performed by using DFT at the B3LYP/6-311+G(d,p) level of theory with the Gaussian 09 program. All results are reported in Table 2 and Figure 3. The electronic distribution and energy levels of the HOMOs and LUMOs (and the corresponding energy gaps, ΔE^{theo}) have been determined on optimised geometries. As expected, all HOMOs are localised at the electron-rich nitrogen centres (IA moieties) thanks to its strong donor character, with theoretical HOMO energy levels lying from −5.59 to −5.84 eV for **SIA-F** (−5.59 eV), **SIA-DAF** (−5.78 eV) and **SIA-TXO$_2$** (−5.84 eV) (Figure 3). These values follow the same trend and are close (0.1 to 0.3 eV) to the HOMO energy levels obtained from electrochemical measurements (−5.48, −5.50 and −5.61 eV for **SIA-F**, **SIA-DAF** and **SIA-TXO$_2$**, respectively; see Figure 4).

The efficient withdrawing effect of DAF and TXO_2 units leads to a localisation of the LUMO only on these backbones in **SIA-DAF** and **SIA-TXO$_2$**. The LUMO energy levels were calculated at −1.84 and −1.56 eV, respectively, following the same trend as that obtained from electrochemical analyses (−2.27 and −2.05 eV, see Figure 4). Compound **SIA-F** displays different behaviour: its LUMO is localised on both F and carbazole (of the IA unit) and lies at −1.36 eV. This explains the large difference between acceptors such as DAF and TXO_2 and "neutral fragments" such as F. The LUMO level calculated for **SIA-F** is higher than those calculated for **SIA-DAF** and **SIA-TXO$_2$**, in accordance with the LUMO levels obtained from electrochemistry (−1.88 eV, see Figure 4).

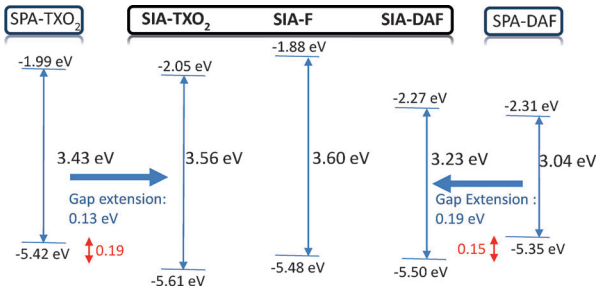

Figure 4. Summary of the HOMO/LUMO energy levels and gap, ΔE^{el}, obtained from electrochemical measurements for SIA derivatives (this work) and SPA derivatives (from ref. [16b]).

Thus, thanks to the D-spiro-A design, compounds **SIA-DAF** and **SIA-TXO$_2$** display a complete spatial separation of their HOMOs and LUMOs. This allows selective tuning of the HOMO and LUMO energy levels (for further efficient charge injections within the device), depending on the strength of the donor/acceptor combination without increasing π conjugation, which dramatically leads to a decrease in E_T.

The theoretical energy gaps, ΔE^{theo}, obtained from theoretical HOMO and LUMO energy levels (Table 2) are 4.23, 3.94 and 4.28 eV for **SIA-F**, **SIA-DAF** and **SIA-TXO$_2$**, respectively; this follows the same trend as that of ΔE^{el}, which has larger gaps for **SIA-F** (3.60 eV) and **SIA-TXO$_2$** (3.56 eV) than that for **SIA-DAF** (3.23 eV). These results are also in accordance with the ΔE^{theo} values previously reported for **SPA-DAF** and **SPA-TXO$_2$**[16b] at 3.77 and 4.13 eV, respectively. Hence, there is a slight gap extension from SPA to SIA compounds due to the lower HOMO level of the latter.

Optical spectroscopy

In cyclohexane, the three compounds present absorption bands between $\lambda = 250$ and 370 nm (see Figure 5, top left). At short wavelengths, each compound presents different absorption bands related to the acceptor units (F, DAF or TXO_2). For **SIA-F**, the classically observed π–π* transitions of the F units in 9,9′-SBF ($\lambda = 257$, 275, 296 and 308 nm)[13a] are visible at $\lambda =$ 275 and 308 nm. For **SIA-DAF**, the bands classically observed for DAF at $\lambda \approx 306$ and 319 nm[15,16b,25] are clearly visible at $\lambda =$ 303 and 317 nm. In **SIA-TXO$_2$**, π-conjugation breaking between the two phenyl units of TXO_2 (through the sulfur atom) leads to the disappearance of the transition observed at $\lambda = 308$ nm in F or at $\lambda = 319$ nm in DAF. However, the weak and broad ab-

sorption band observed at $\lambda = 310$ nm may indicate slight π conjugation between the phenyl units in TXO_2.

At higher wavelengths, the three compounds present two similar weak absorption bands with maxima at $\lambda = 339$ and 355 nm for **SIA-F**, $\lambda = 338$ and 355 nm for **SIA-DAF** and $\lambda = 338$ and 352 nm for **SIA-TXO$_2$**. These weak bands are attributed to the n–π^* transitions of the SIA units. As a result, the ΔE^{opt} values of **SIA-F**, **SIA-TXO$_2$** and **SIA-DAF** are almost identical (3.41/3.42 eV) and are in the same range as those reported in the literature for other SIA derivatives ((3.40 ± 0.1) eV).[23, 17a, d] As observed by Liao et al. for the series of **SCzDBT4**/**STDBT4** and **SCzDBT2**/**STDBT2** (Scheme 2),[23] the ΔE^{opt} values of **SIA-TXO$_2$** and **SIA-DAF** are smaller than those of **SPA-TXO$_2$** and **SPA-DAF**[16b] (by 0.1 eV for the TXO_2 series and by 0.21 eV for the DAF series). These results are in complete contradiction to the gap modulations obtained through electrochemical studies or through theoretical calculations, which show an increase of the gap from SPA to SIA derivatives. This divergence between optical and electrochemical or theoretical tendencies may be explained by the fact that the absorption bands at low energy are related to transitions involving only the SIA units and do not reflect the HOMO/LUMO difference. This important characteristic of D-spiro-A molecules is explained below through time-dependant TD-DFT investigations.

Indeed, TD-DFT calculations performed at the B3LYP/6-311 + G(d,p) level of theory with the Gaussian 09 program shed light on these features (Figure 6). Thus, in **SIA-F**, we note that the main transition is a HOMO/LUMO transition (88 %, $\lambda =$ 339.87 nm, $f = 0.049$, excited state 1) with a significant mixing of the orbitals. Compounds **SIA-TXO$_2$** and **SIA-DAF** display different behaviour due to their stronger acceptor units. Indeed, in **SIA-TXO$_2$**, we note that the first excited state mainly possesses a HOMO/LUMO + 1 contribution (82 %, $\lambda = 331.77$ nm, $f = 0.0201$, excited state 1); both orbitals are centred on the IA unit, and thus, are without any charge-transfer character. We note that the HOMO/LUMO transition possesses only a very weak contribution (13 %) due to the spatial separation of HOMO and LUMO. The main transition for **SIA-TXO$_2$** is a HOMO/LUMO + 2 transition (92 %, $\lambda = 326.86$ nm, $f = 0.0708$, excited state 3). In **SIA-DAF**, the first excited state ($\lambda =$ 366.46 nm, excited state 1) is related to a HOMO/LUMO transition; however, with a very weak oscillator strength ($f = 0.005$). Because the HOMO and LUMO are centred on the IA and DAF fragments, respectively, this transition possesses a strong charge-transfer character. Indeed, due to the orthogonal configuration of D-spiro-A compounds, this HOMO/LUMO transition should occur through space, and hence, is theoretically forbidden and not observed experimentally. However, we note that the main transition (excited state 2) is a HOMO/LUMO + 1 transition ($\lambda = 336.19$ nm, $f = 0.0527$); both orbitals are centred on the IA unit. This behaviour is identical to that exposed above for **SIA-TXO$_2$**. Thus, both **SIA-DAF** and **SIA-TXO$_2$** possess

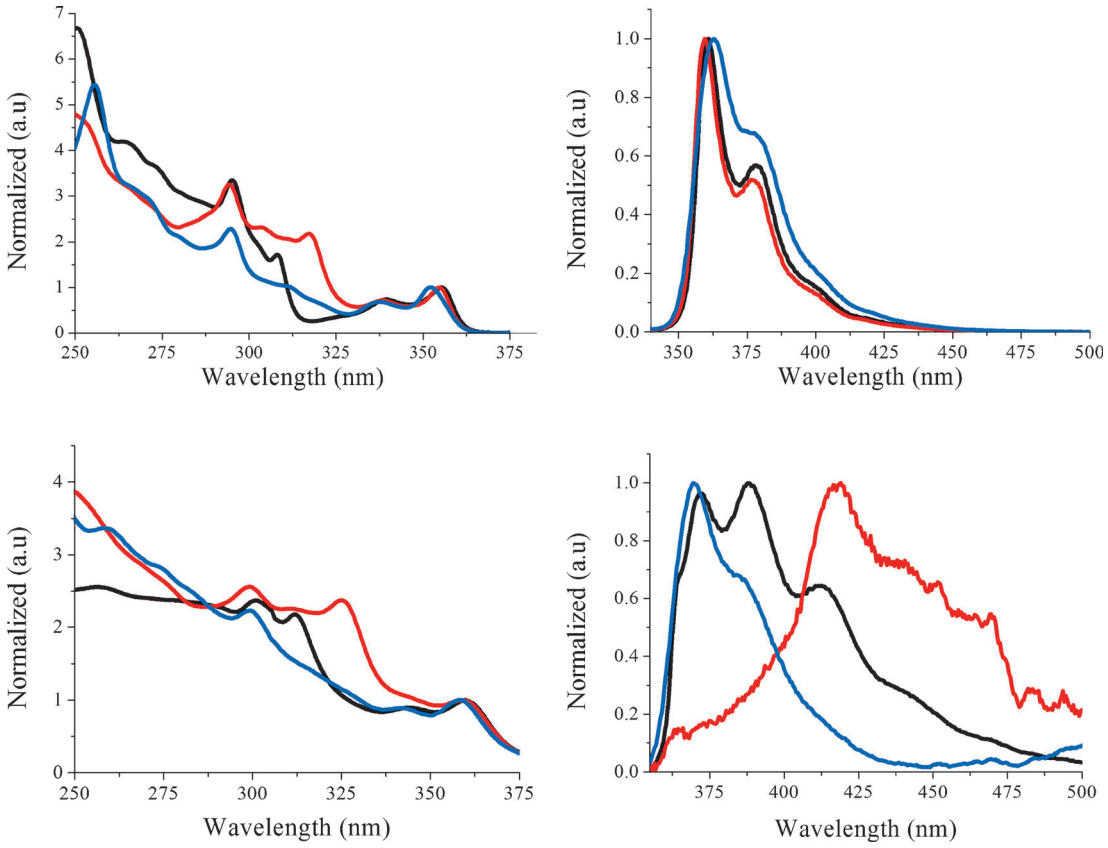

Figure 5. Optical properties of **SIA-F** (black line), **SIA-TXO$_2$** (blue line) and **SIA-DAF** (red line). Top left: UV/Vis absorption in cyclohexane; top right: photoluminescence (PL) spectra in cyclohexane at room temperature ($\lambda_{exc} = 295$ nm); bottom left: solid-state UV/Vis absorption; bottom right: solid-state PL spectra of thin films of SIA derivatives obtained by spin coating from solutions in THF (10 mg mL^{-1}).

a main transition at $\lambda \approx 332/336$ nm (HOMO/LUMO + 1 transition with $f = 0.02$ for the former and $f = 0.05$ for the latter), similar to that found in **SIA-F** (HOMO/LUMO transition, $\lambda = 339.9$ nm with $f = 0.049$). This is in accordance with the experimental spectra, which display the main band at $\lambda = 340$ nm with almost identical molar absorption coefficients ($\varepsilon = 6000$, 6000 and 5000 $L\,mol^{-1}\,m^{-1}$ at $\lambda = 339$, 338 and 338 nm for **SIA-F**, **SIA-DAF**, and **SIA-TXO$_2$**, respectively; Table 3).

Table 3. Photophysical properties of the three dyes.

	SIA-F	SIA-DAF	SIA-TXO$_2$
λ_{max}^{abs} solution[a] [nm]	295, 308, 339, 355	294, 303, 317, 338, 355	295, 310(s), 338, 352
ε[a] (10^4, $L\,mol^{-1}\,M^{-1}$)	2.6, 1.5, 0.6, 0.7	2.8, 2.1, 2.0, 0.6, 0.8	1.8(s), 0.5, 0.7
λ_{max}^{abs} thin film[b] [nm]	301, 312, 344, 360	299, 310, 325, 359	299, 342, 358
λ_{max}^{fluo} solution[a] [nm]	361, 378	360, 377	363, 379
λ_{max}^{fluo} thin film[b] [nm]	372, 388, 412	418(b)	370, 384
QY[c] [%]	33	38	39

[a] Measured in cyclohexane. [b] Obtained from a solution in THF at 10 $g\,L^{-1}$. [c] Calculated from a solution of quinine sulfate in 1 N sulfuric acid, (s): shoulder, (b): broad.

Thus, the main band at $\lambda \approx 352/355$ nm observed in the experimental spectra of the three dyes is related to a transition mainly involving only the IA unit. This feature explains the identical ΔE^{opt} values of the three dyes. This is an important characteristic of the present IA-based molecules (different to their PA analogues) and will also have important consequences on other optical properties (e.g., quantum yield (QE), solvatochromism; see below).

Another remarkable feature is related to the comparison of the absorption spectra of SIA derivatives described herein and those of SPA analogues.[16b] Thus, both **SPA-DAF** and **SPA-TXO$_2$** possess main bands at $\lambda = 319$ and 323 nm, respectively; these are significantly blueshifted relative to those of their SIA counterparts (at $\lambda \approx 350$ nm, see above). Because the HOMOs of SIA derivatives obtained from electrochemistry (Figure 4) are deeper than those of SPA derivatives, and because the LUMO is almost identical for **SPA-DAF/SIA-DAF** (−2.31/−2.27 eV) and **SPA-TXO$_2$/SIA-TXO$_2$** (−1.99/−2.05 eV), we expected the gap of SIA derivatives to be larger than those of SPA derivatives, as observed by electrochemistry. Nevertheless, the opposite is observed from optical measurements ($\Delta E^{opt} = 3.4$ eV for both **SIA-TXO$_2$/SIA-DAF**, 3.54 eV for **SPA-TXO$_2$** and 3.64 eV for **SPA-DAF**). This can be explained by the above-mentioned features because the HOMO/LUMO transitions are never observed in such D-spiro-A systems and the value of ΔE^{opt} does not reflect the HOMO/LUMO difference. In addition, these are not the same transitions that are involved in the last band of the absorption spectra. Indeed, for **SIA-DAF** and **SIA-TXO$_2$**, we have shown above that the main transitions are those of HOMO/LUMO + 1 and HOMO/LUMO + 2, respectively; both involve only the IA core. For **SPA-DAF**,[16b] the blueshifted band observed in the experimental spectrum is a HOMO-1/LUMO transition that involves only the DAF units and, for **SPA-TXO$_2$**,[16b] these are HOMO/LUMO + 1 and HOMO/LUMO + 5 transitions that involve both PA and TXO_2 units. This important characteristic is a common feature of D-spiro-A compounds, in which the strength of the donor and that of the acceptor can drastically change the transitions involved, and hence, the complete optical properties.

The emission spectra of the three SIA derivatives in cyclohexane all present similar shapes with two bands at $\lambda \approx 360$ and 377 nm and very weak emission bands at $\lambda \approx 400$ and 425 nm (see Figure 5, top right). These well-resolved spectra with maxima at $\lambda = 361$, 360 and 363 nm for **SIA-F**, **SIA-DAF** and **SIA-TXO$_2$**, respectively, are the mirror images of the corresponding absorption spectra with Stokes shifts ($\lambda_{em} - \lambda_{abs}$ in nm) of 6, 5 and 11 nm, respectively. The emission spectra present the same shape as that reported in the literature for structurally related compounds **SFCA** and **SFCC**,[17e] **SCzDBT2** and **SCzDBT4**,[23] **SPCPO1** and **SPCPO2**,[17a] and **BIPIA**[17b] (see struc-

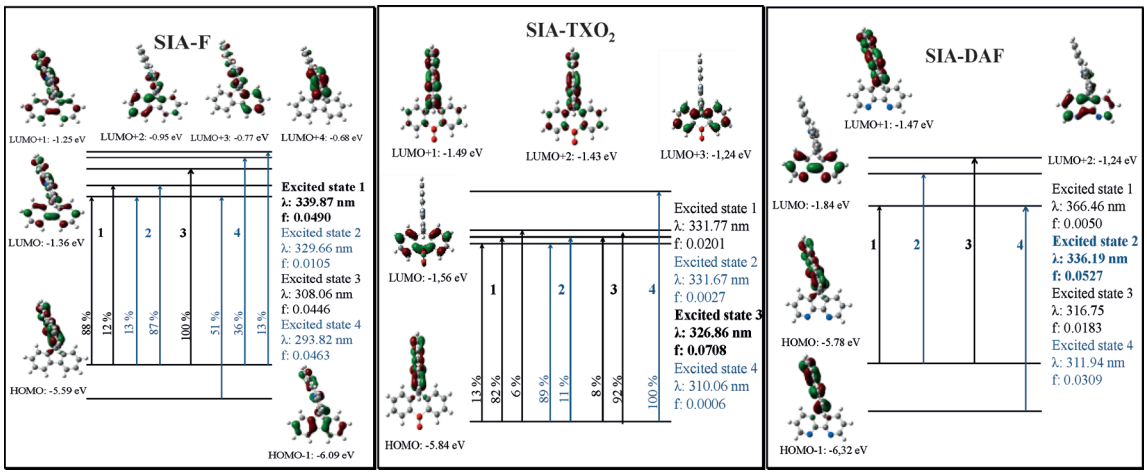

Figure 6. Frontier molecular orbitals calculated by DFT (B3LYP/6-311 + G(d,p)) and the first four electronic transitions calculated by TD-DFT after geometry optimisation with DFT (B3LYP/6-311 + G(d,p)), shown with an isovalue of 0.04 e $bohr^{-3}$; the main transition is given in bold.

tures in Scheme 2); the shape is typical of the emission of the fused carbazole core of the SIA derivatives. The small Stokes shifts are consistent with the high rigidity of the present D-spiro-A derivatives. In addition, the emission QYs (in solution relative to quinine sulfate) have been calculated to be between 33 and 39% (**SIA-F**: 33%, **SIA-DAF**: 38% and **SIA-TXO$_2$**: 39%). These relatively high and similar QYs clearly confirm that the emissions are almost integrally due to transitions within the IA unit (see the TD-DFT discussion above). Indeed, in such D-spiro-A compounds, very low QYs are usually observed when the HOMO and LUMO are spatially separated, leading to forbidden (or very disfavoured) through-space optical transitions.[16b] Thus, the corresponding PA dyes, **SPA-DAF** and **SPA-TXO$_2$**, possess an unstructured emission spectrum with a corresponding very low QY (0.1 and 4.1%, respectively), which is characteristic of photoinduced intramolecular charge transfer (ICT).[16b] Thus, the rigidification of the donor unit in D-spiro-A compounds significantly increase the QY of the resulting dyes.

In the solid state, the absorption spectra (Figure 5, bottom left) remain similar to those recorded in solution, with only a redshift of 5 nm. Such similarity between absorption spectra in solution and in the solid state clearly indicates that there are very weak intermolecular interactions in the ground state in thin films. Regarding the solid-state fluorescent properties (Figure 5, bottom right) for **SIA-F** and **SIA-TXO$_2$**, only a small redshift is observed between solution and thin-film emissions (10 nm for **SIA-F** and 6 nm for **SIA-TXO$_2$**); this again indicates weak interactions in the excited state. The solid-state fluorescent spectrum of **SIA-DAF** nevertheless appears poorly resolved, with a very weak emission at $\lambda = 364$ nm and a broad ill-defined band at $\lambda \approx 418$ nm.

Studying the absorption and emission spectra of bipolar compounds in different polarity solvents is a key point to assess the intensity of charge transfer and the polarity of the excited states (Figure 7). Thus, we first note that the absorption maxima of **SIA-F** are almost insensitive to the dielectric constant of the environment, with only a slight blueshift of the maximum from cyclohexane ($\lambda_{max} = 355$ nm) to acetonitrile ($\lambda_{max} = 352.5$ nm). This very weak effect is due to a slight gap extension caused by stabilisation of the ground state in acetonitrile. As classically observed, the emission spectra are more influenced by the polarity of the solvent, although this influence remains modest herein. Indeed, we note that the emission of **SIA-F** is redshifted by only 10 nm from cyclohexane ($\lambda_{max} = 361$ nm) to acetonitrile ($\lambda_{max} = 371$ nm). In addition, the QYs are not affected by the solvent polarity (33% in cyclohexane, 32% in acetonitrile, see Table S6 in the Supporting Information). These data indicate that **SIA-F** displays a very weak photoinduced ICT due to the significant mixing of both HOMO and LUMO levels (Figure 6). Using Lippert–Mataga formalism (see the Supporting Information for details; the radius of the molecule has been estimated from crystallography results), one can evaluate the dipole moment difference, $\Delta\mu$, between the ground and first excited state. For **SIA-F** (dipole moment at the ground state obtained from DFT calculations: $\mu(S^0) = 0.6$ D), a small $\Delta\mu$ of 8.66 D is calculated in accordance with the weak solvatochromic effect observed in emission; $\mu(S^1)$ is therefore estimated to be 9.3 D.

The case of **SIA-TXO$_2$** is very similar to that of **SIA-F**, due to the weak acceptor strength of the TXO_2 fragment, with a shift of the absorption bands of less than 2 nm and a shift of the emission bands of less than 10 nm; however, there is a decrease in the emission QYs, which is halved upon going from that in a non-polar solvent (40% in cyclohexane) to a more polar one (20% in acetonitrile; see Table S6 in the Supporting Information). The dipole moment of **SIA-TXO$_2$** in the ground state, $\mu(S^0) = 5.7$ D, obtained through DFT calculations is much higher than that of **SIA-F** ($\mu(S^0) = 0.6$ D). For **SIA-TXO$_2$**, a small $\Delta\mu$ of 6.23 D is therefore calculated through Lippert–Mataga formalism, and $\mu(S^1)$ is therefore estimated to be 11.9 D. Hence, there is only a very weak solvatochromic effect, which translates into weak photoinduced ICT within **SIA-TXO$_2$**. This feature confirms the significant overlap between the orbitals involved in the transitions responsible for these emission processes (HOMO/LUMO + 1 transition only involving the IA fragment).

As observed for the other molecules, the absorption spectra of **SIA-DAF** are not dependent on the solvent polarity and follow exactly the same trend as those exposed above for **SIA-TXO$_2$** and **SIA-F** (cyclohexane: $\lambda_{max} = 354.5$ nm and acetonitrile: $\lambda_{max} = 353$ nm). The dipole moment at the ground state obtained through DFT calculations ($\mu(S^0) = 4.1$ D) is intermediate between those of **SIA-F** and **SIA-TXO$_2$**. However, the emission spectra of **SIA-DAF** display peculiar behaviour. Indeed, from cyclohexane to ethyl acetate, only a very weak redshift of 10 nm is detected (cyclohexane: $\lambda_{max} = 360$ nm and ethyl acetate: $\lambda_{max} = 370$ nm). This feature is also indicative of weak photoinduced ICT in these solvents, in accordance with transitions between molecular fragments only involving the IA unit. This is consistent with the conclusions drawn from TD-DFT results and absorption spectra. However, in acetonitrile, a dual emission is observed. Indeed, the first structured emission is clearly observed at $\lambda = 360$ nm, which is at exactly the same wavelength as that observed in cyclohexane. In addition, a new and very broad emission band between $\lambda = 400$ and 550 nm (centred at $\lambda = 453$ nm) is also recorded in acetonitrile. The QYs also drop from 38% in cyclohexane to 5% in toluene, 1% in THF, 1.5% in ethyl acetate and 1% in acetonitrile (see Table S6 in the Supporting Information). Hence, we believe that the first emission corresponds to a locally excited state of the SIA unit and the second broad band to a photoinduced ICT excited state from the two fragments: IA (HOMO) to DAF (LUMO).

For **SIA-DAF**, the Lippert–Mataga calculations were performed separately for these two excited states. In addition, and in the absence of the crystallographic structure of **SIA-DAF**, the radius of this molecule is expected to be 7.0 Å, similar to that of **SIA-F** and **SIA-TXO$_2$**. Because the radius of these molecules is directed by the SIA core (Figure 1), this estimation is expected to be correct. For the locally excited state, the dipole moment at the excited state, $\mu(S^1)_{LE}$, is 9.08 D, which is similar to that calculated for **SIA-F** (9.26 D) and shows that the acceptor core has no influence on the emissive properties of this locally excited state (SIA unit). The ICT excited state,

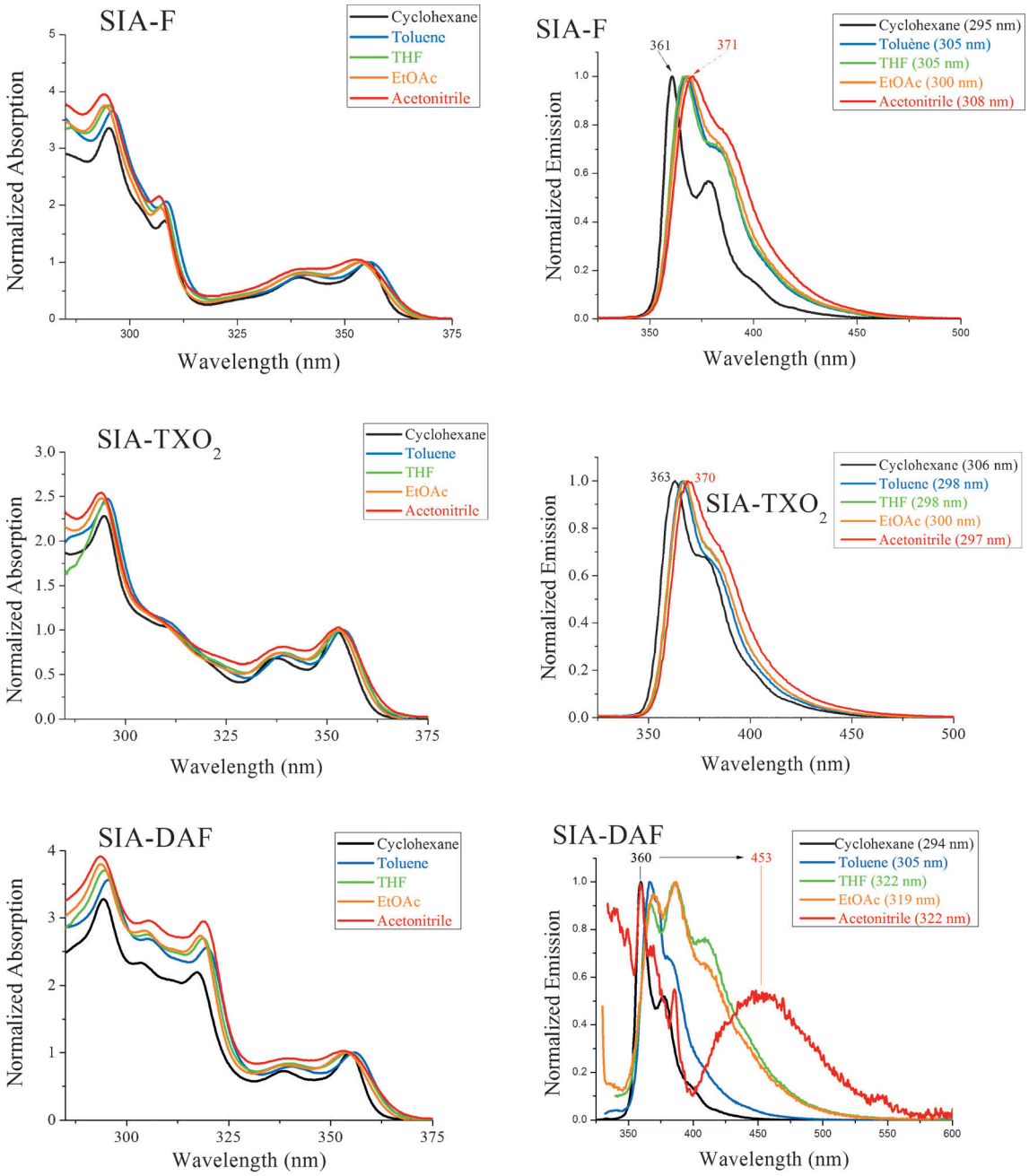

Figure 7. Absorption (left) and emission (right) spectra of **SIA-F** (top), **SIA-TXO$_2$** (middle) and **SIA-DAF** (bottom) in different solvents (cyclohexane: black, toluene: blue, THF: green, ethyl acetate: orange, acetonitrile: red).

$\mu(S^1)_{ICT}$ of **SIA-DAF** has been calculated for only two solvents (cyclohexane and acetonitrile). Thus, compound **SIA-DAF** displays a large $\Delta\mu$ of 25.56 D, leading to a $\mu(S^1)$ of 29.65 D. In summary, increasing the solvent polarity leads to the appearance of a new emission band that is characteristic of an ICT excited state, which is stabilised relative to the ground state.

Finally, to examine the suitability of the three dyes as host materials for a high E_T phosphorescent dopant, the phosphorescence contribution of the molecules was recorded at 77 K (Figure 8). From these spectra, the E_T values were calculated from the lowest phosphorescent band at 2.87, 2.89 and 2.93 eV for **SIA-F**, **SIA-DAF** and **SIA-TXO$_2$**, respectively. These E_T values follow the same trend as that obtained from theoretical calculations (2.94, 2.97 and 2.98 eV, respectively; Table 2). Compared with the SPA counterparts, SIA compounds present E_T values that are lower by 0.09 and 0.15 eV ($E_T = 2.98$ eV for **SPA-DAF** and 3.08 eV for **SPA-TXO$_2$**). Interestingly, the E_T values of the three compounds are similar to those reported in the literature for other SIA derivatives, but remain slightly lower than that of carbazole (3.02 eV).[26] Thus, we note that **BIPIA**,[17b] **SPCPO1** and **SPCPO2**[17a] (see structures in Scheme 2) possess an E_T value of 2.95 eV, which is almost identical to that of **SIA-TXO$_2$** and can be tentatively assigned to the E_T of IA (TXO_2 should indeed possesses a higher E_T value due to π-conjuga-

tion breaking induced by SO_2 between the two phenyl units). It is nevertheless difficult to assign with complete certainty which fragment drives the E_T because, for example, compound **9,9′-SBF** possesses an E_T of 2.87 eV,[13a] which is identical to that of **SIA-F** and very similar to that of **SIA-DAF**. However, it is clear that the E_T of IA remains very high, which is an important feature for the future design of host materials based on this fragment. This also highlights that the present design strategy is very efficient at maintaining a high E_T value as well as tuning of the HOMO/LUMO levels.

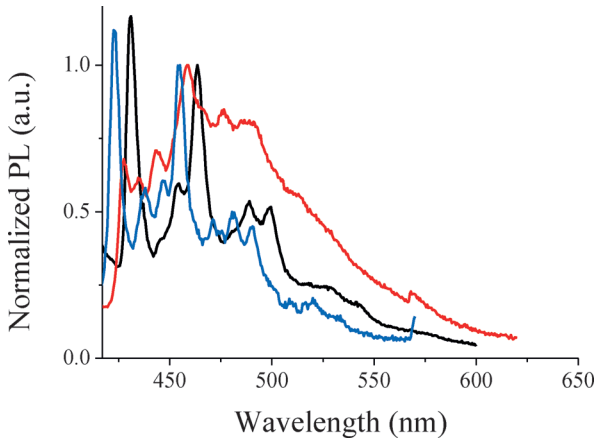

Figure 8. PL spectra of **SIA-F** (black), **SIA-TXO$_2$** (blue) and **SIA-DAF** (red) recorded in a frozen matrix of 2-methyltetrahydrofuran at 77 K (λ_{exc} = 310 nm for **SIA-F**, λ_{exc} = 285 nm for **SIA-TXO$_2$** and 315 nm for **SIA-DAF**).

Phosphorescent OLEDs

Compounds **SIA-DAF** and **SIA-TXO$_2$** have been used as hosts for green [Ir(ppy)$_3$] (ppy = 2-phenylpyridinato-C^2,N) and sky-blue FIrpic dopants. [Notably, compound **SIA-F** has not been tested in green and blue PhOLEDs because F is not an efficient acceptor unit.] The EML was inserted between indium tin oxide (ITO)/CuPc (10 nm; Pc = phthalocyanine)/*N*,*N*′-di(1-naphthyl)-*N*,*N*′-diphenyl-[1,10-biphenyl]-4,4′-diamine (NPB; 40 nm)/4,4′,4″-tris(carbazol-9-yl)triphenylamine (TCTA; 10 nm) on the anode side and 1,3,5-tris(1-phenyl-1*H*-benzimidazol-2-yl)benzene (TPBI; 40 nm)/LiF (1.2 nm)/Al (100 nm) on the cathode side. To properly compare the efficiency of different hosts, the architecture of the device first used herein is the same as that used for **SPA-DAF** and **SPA-TXO$_2$**.[16] Indeed, it is important to stress that changing the device architecture can drastically change the device performance and it is therefore not possible to evaluate the efficiency of a host material. ITO is used as the anode, CuPc is the hole injecting layer, NPB is the hole transporting layer, TCTA is the electron/exciton blocking layer, TPBI is both the electron transporting layer (ETL) and the hole blocking layer (HBL), and a thin film of lithium fluoride covered with aluminium is the cathode.

A comparison of the different green PhOLEDs performances (Table 4 and Figure S57 in the Supporting Information) shows that the best performance is recorded with **SIA-TXO$_2$** as a host with 10% [Ir(ppy)$_3$]. This device emits light at a low voltage of 3.1 V and reaches a high EQE of 22.8% with a CE as high as 62.7 cd A^{-1} and a PE of 36.8 Lm W^{-1} (both recorded at 1 mA cm^{-2}). The EQE of **SIA-TXO$_2$** appears to be higher than that recorded with the PA analogue, **SPA-TXO$_2$** (EQE = 19.5% under identical experimental conditions).[16a] Thus, the rigidification of the donor (IA versus PA) in D-spiro-A compounds is highly beneficial to improve the device performance with green phosphorescent emitters. This clearly highlights the high potential of the IA unit for such applications.

Green devices with **SIA-DAF** as a host present an EQE reaching 16.6% (CE = 47.7 cd A^{-1} and PE = 31.5 Lm W^{-1} both recorded at 1 mA cm^{-2}); hence, this is less efficient than the devices with **SIA-TXO$_2$**. This feature indicates that the TXO_2 acceptor is more efficient in such devices than the DAF acceptor. Because the LUMO level of DAF is lower than that of TXO_2, this feature indicates that electron injection is not directly linked to this difference in performance. Similar conclusions have been drawn with PA derivatives.[16b] In addition, at low current density, we note that **SIA-DAF** (< 1 mA cm^{-2}; Table 4) leads to a lower maximum EQE than that reported with the **SPA-DAF** analogue (16.6 versus 19.2%, respectively), but at a higher current density, namely, 10 mA cm^{-2}, the EQE values are almost identical (12.9 versus 12.2%).

All devices with IA derivatives as the host emit light at a higher voltage (2.8–3.1 V) than those with PA derivatives as the host (2.5–2.6 V). The gaps of the IA derivatives are larger than those of the PA derivatives (increase in the gap of 0.13 eV between **SPA-TXO$_2$** and **SIA-TXO$_2$** and 0.19 eV between **SPA-DAF** and **SIA-DAF**), with notably a lower HOMO level, so charge injection in the EML may be more difficult than that in the PA-derived hosts, which may explain the increase in the threshold voltages.

Table 4. Selected electroluminescence (EL) data of the green devices.[a]

EML	V_{on} [V]	CE [cd A^{-1}]		PE (lm W^{-1})		EQE [%]		CIE (x,y)	L_{max} [cd m^{-2}]
	L = 1[b]	J = 1[c]	J = 10[c]	J = 1[c]	J = 10[c]	J = 10[c]	Max (J[c])	J = 10	(J[c])
SIA-TXO$_2$ + 10% [Ir(ppy)$_3$][d]	3.1	62.7	58.7	36.8	27.4	16.4	22.8 (0.06)	0.32,0.63	50845 (190)
SIA-TXO$_2$ + 20% [Ir(ppy)$_3$][d]	3.0	52.6	51.7	31.3	24.1	14.5	15.0 (2.10)	0.32,0.63	35240 (180)
SPA-TXO$_2$ + 9% [Ir(ppy)$_3$][e]	2.5	60.7	54.5	38.3	26.2	14.8	19.5 (0.05)	0.30,0.63	35518 (130)
SIA-DAF + 10% [Ir(ppy)$_3$][d]	2.8	47.7	46.8	31.5	23.4	12.9	16.6 (0.05)	0.32,0.63	37492 (160)
SPA-DAF + 10% [Ir(ppy)$_3$][f]	2.6	45.6	42.7	31.4	22.4	12.2	19.2 (0.01)	0.34,0.63	31675 (130)

[a] CE = current efficiency, PE = power efficiency. [b] In cd m^{-2}. [c] In mA cm^{-2}. [d] This work. [e] From ref. [16a]. [f] From ref. [16b].

An increase in the amount of [Ir(ppy)$_3$] in **SIA-TXO$_2$** (10 to 20%) leads to a significant decrease in the device performances ($EQE_{10\%}$ = 22.8% versus $EQE_{20\%}$ = 15%) and may be attributed to triplet-energy annihilation in the presence of a higher amount of dopant.

The luminance maximum of IA-based PhOLEDs (37492 cd m^{-2} with **SIA-DAF** and 50845 cd m^{-2} with **SIA-TXO$_2$**) is very high, and higher than that of PA-based PhOLEDs (31675 cd m^{-2} with **SPA-DAF** and 35518 cd m^{-2} with **SPA-TXO$_2$**);[16b] this again highlights the potential of the IA core for such applications.

Finally, the EL spectra of the devices (see Figure S57 in the Supporting Information) only present the emission of the green dopant (CIE: 0.32, 0.63), which corresponds to efficient energy transfers between the host and guest.

As shown in Figure 9 and summarised in Table 5, the PhOLED with **SIA-TXO$_2$** as the host and the sky-blue emitter FIrpic (10%) reaches a high EQE of 9.7%, whereas those with **SIA-DAF** are much less efficient, reaching an EQE of only 6.2%. The CE and PE (at 1 mA cm^{-2}) values are evaluated to be 23.5 cd A^{-1} and 14.3 lm W^{-1}, respectively, for **SIA-TXO$_2$** and 15.5 cd A^{-1} and 11.1 lm W^{-1}, respectively, for **SIA-DAF**. The corresponding EL spectra were nevertheless very different. Indeed, the EL spectra of **SIA-TXO$_2$**-based PhOLEDs (Figure 10, bottom) only display the emission of FIrpic (CIE: 0.19,0.44) without any unwanted emission at lower wavelengths, which indicates the efficiency of energy transfers. These spectra are independent of the current density and prove the high stability of the EL in these devices. Compound **SIA-DAF** displays very different behaviour (Figure 10, top). Indeed, although the EL spectra at low current density, 30/60 mA cm^{-2}, are very similar to those presented for **SIA-TXO$_2$**-based PhOLEDs (CIE: 0.22,0.45), increasing the current density to 90 mA cm^{-2} leads to a modification of the EL spectra (decrease in the emission band at λ = 475 nm at the expense of an increase in the emission at λ = 560 nm, as shown in the non-normalised spectrum; Figure S58 in the Supporting Information), which shows the instability of the **SIA-DAF**-based PhOLEDs. We believe that this instability can be attributed to the DAF fragment, which also possesses an unusual PL spectrum in the solid state (Figure 5, bottom right). Additional experiments are needed to clearly explain the influence of the **SIA-DAF** host on the EL spectra of the blue PhOLED devices (e.g., influence of the doping level, thickness of the layer).

Increasing the amount of FIrpic (20%) in **SIA-TXO$_2$**-based PhOLEDs leads to an increase in the maximum EQE to 10.7%, with maximum CE and PE values recorded at 27.9 cd A^{-1} and at 16.0 Lm W^{-1}, respectively. The EQE of **SIA-TXO$_2$** is in the same range than that recorded for the PA analogue **SPA-TXO$_2$** (EQE: 11%), with nevertheless an impressive increase in the CE at 1 mA cm^{-2} (27.9 versus 17.2 cd A^{-1}) for **SIA**- vs **SPA-TXO$_2$** respectively).

As a result of the promising performances of **SIA-TXO$_2$**, we modified the device architecture to enhance the device efficiency by using a different ETL. Reports in the literature provide examples of increasing the device efficiency by using TmPyPB[27] as the ETL and HBL instead of TPBI.[28] TmPyPB has

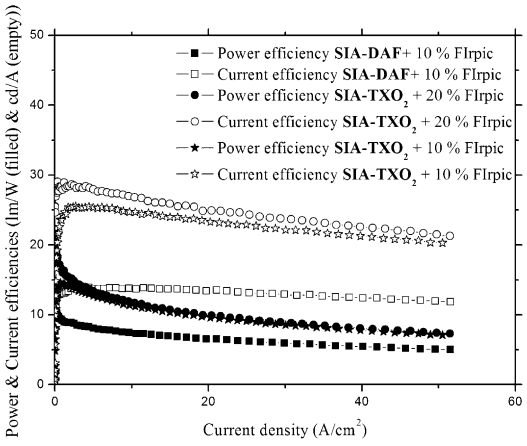

Figure 9. CEs (open symbols) and PEs (filled symbols) versus the current density of the blue devices with **SIA-DAF** doped with 10% FIrpic (squares) and **SIA-TXO$_2$** doped with 10 (stars) or 20% (circles) FIrpic as the EML.

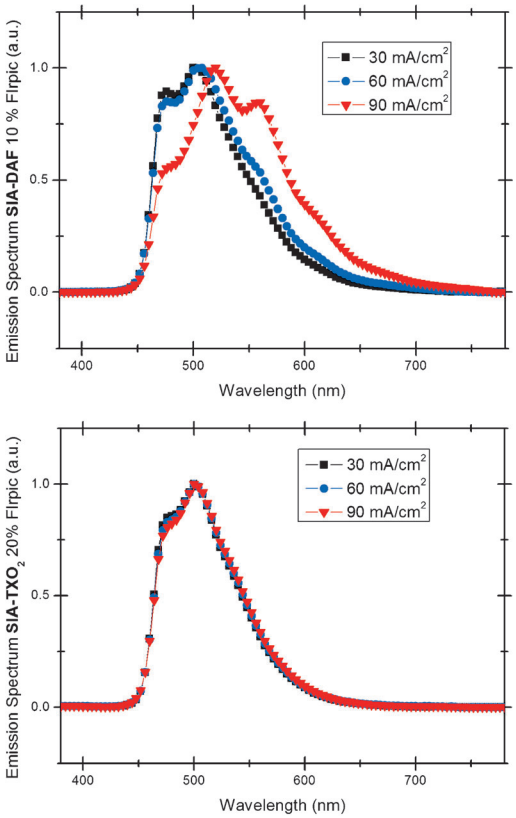

Figure 10. EL spectra of **SIA-DAF** + 10% FIrpic (top) and **SIA-TXO$_2$** + 20% FIrpic (bottom) recorded at different current densities of 30 (black), 60 (blue) and 90 mA cm^{-2} (red).

a higher E_T (2.78 eV) than that reported for TPBI (2.7 eV), which may lead to a better confinement of the triplet excitons in the EML. Thus, with the device architecture ITO/CuPc/NPB/TCTA/EML/TmPyPB/LiF/Al, an EQE as high as 14.08% at 0.5 mA cm^{-2} (Figure 11) with a corresponding CE of 30.6 cd A^{-1} (EQE = 12.73% at 10 mA cm^{-2}, CE = 27.67 cd A^{-1}) is obtained. As a result of the increase in device performance (by changing TPBI to TmPyPB as the ETL/HBL layer), we are confident that

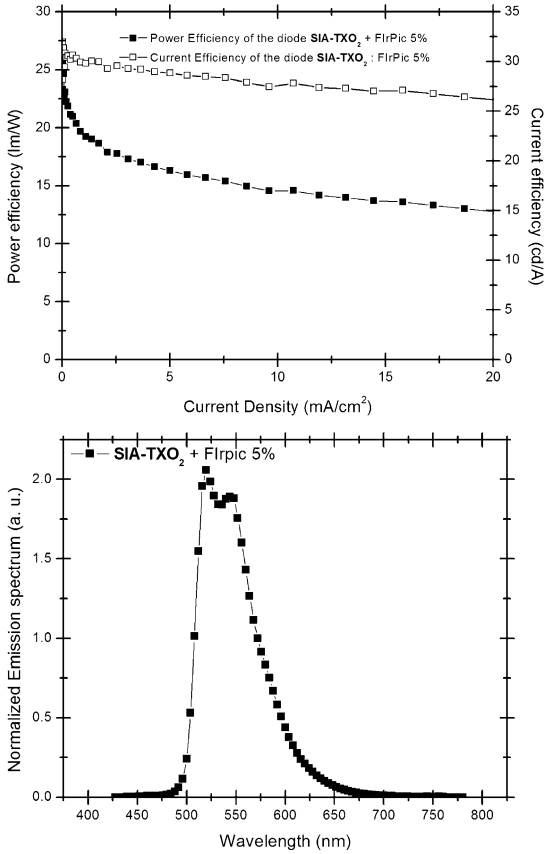

Figure 11. CE (open symbols) and PE (filled symbols) versus the current density of sky-blue devices with **SIA-TXO$_2$** doped with 5% FIrpic as the EML and 1,3,5-tri[(3-pyridyl)phen-3-yl]benzene (TmPyPB) as the ETL/HBL (top; device architecture: (ITO/CuPc/NPB/TCTA/EML/TmPyPB/LiF/Al) and corresponding EL spectrum recorded at 10 mA cm^{-2} (bottom).

the device performances may be boosted even more by fine-tuning the different layers surrounding the host–guest EML. Such a refinement of the device architecture has unfortunately not been done in the present study, but will be investigated in the future.

Conclusion

We reported a detailed structure–property relationship study of a series of efficient host materials for green and sky-blue PhOLEDs based on the D-spiro-A design. In this work, we investigated the association of the IA unit connected through a spiro bridge to different acceptor units, namely, the F, TXO_2 or DAF moieties. These host materials can be easily synthesised through a short, efficient, low-cost and highly adaptable synthetic route by using common intermediates, which is a key point for mass production. The dyes possess a high E_T, and tuneable HOMO/LUMO levels, depending on the strength of the donor/acceptor combination. The peculiar electrochemical and optical properties of the IA moiety have been investigated in detail through a comparison with the PA counterparts. We have shown that the rigidification of the donor group has a strong impact on the electronic properties, and IA derivatives display very different properties from those of the PA derivatives (e.g., optical transitions, QY). Finally, these molecules have been incorporated as hosts in green and sky-blue PhOLEDs. For **SIA-TXO$_2$** as a host, EQE values as high as 23 and 14% have been obtained for green and sky-blue PhOLEDs, respectively. We have also shown that, in some cases, IA-based hosts can be more efficient than the known and highly efficient PA counterparts. We believe that the D-spiro-A design is promising to produce very efficient host materials for blue PhOLEDs, and that the IA fragment can have a brilliant future in such applications.

Acknowledgements

We wish to thank the CDIFX (Rennes) for X-ray diffraction data, the C.R.M.P.O (Rennes) for mass analyses, GENCI for allocation of computing time under project c2015085032 (Dr. F. Barrière, Rennes), the Institut des Sciences Analytiques (Villeurbanne) for TGA, the Service de Microanalyses-CNRS (Gif sur Yvette) for CHN analyses, S. Fryars (Rennes) for technical assistance and Dr Z. Jiang (Soochow University) for helpful discussions. We wish to warmly thank the ANR Project *HOME-OLED* (no. 11-BS07-020-01) for a studentship (ST) and the ANR project *Men In Blue (*ANR-14-CE05-0024) for financial support.

Keywords: donor–acceptor systems · electrochemistry · luminescence · spiro compounds · structure–activity relationships

[1] a) J.-H. Jou, S. Kumar, A. Agrawal, T.-H. Li, S. Sahoo, *J. Mater. Chem. C* **2015**, *3*, 2974 – 3002; b) H. Sasabe, J. Kido, *Chem. Mater.* **2011**, *23*, 621 – 630; c) J. Shinar, R. Shinar, *J. Phys. D* **2008**, *41*, 133001.

[2] a) L. Xiao, Z. Chen, B. Qu, J. Luo, S. Kong, Q. Cong, J. Kido, *Adv. Mater.* **2011**, *23*, 926 – 952; b) Y. Tao, C. Yang, J. Qin, *Chem. Soc. Rev.* **2011**, *40*, 2943 – 2970; c) H. Sasabe, J. Kido, *Eur. J. Org. Chem.* **2013**, *34*, 7653 –

Table 5. Selected EL data of the blue devices.

EML	V_{on} [V]	CE [cd A^{-1}]		PE [lm W^{-1}]		EQE [%]		CIE (*x,y*)	L_{max} [cd m^{-12}]
	$L=1$[a]	$J=1$[b]	$J=10$[b]	$J=1$[b]	$J=10$[b]	$J=10$[b]	Max (J[b])	$J=10$	(J[b])
SIA-TXO$_2$ + 10% FIrpic	3.2	23.5	24.7	14.3	11.4	9.4	9.7 (2.69)	0.19,0.44	8733 (100)
SIA-TXO$_2$ + 20% FIrpic	3.2	27.9	26.9	16.0	11.8	9.9	10.7 (0.38)	0.19,0.45	9255 (90)
SPA-TXO$_2$ + 20% FIrpic	3.1	17.2	27.0	12.7	14.3	10.5	11.0 (3.47)	0.17,0.42	9200 (90)
SIA-DAF + 10% FIrpic	3.1	13.1	13.7	9.1	7.5	6.0	6.2 (3.07)	0.22,0.45	4328 (80)
SPA-DAF + 20% FIrpic	2.9	22.0	24.6	16.6	14.2	10.2	10.2 (7.80)	0.19,0.43	6100 (70)

[a] In cd m^{-2}. [b] In mA cm^{-2}.

7663; d) D. Chen, S.-J. Su, Y. Cao, *J. Mater. Chem. C* **2014**, *2*, 9565 – 9578; e) X. Yang, G. Zhou, W.-Y. Wong, *Chem. Soc. Rev.* **2015**, *44*, 8484 – 8575.

[3] a) C. Adachi, M. A. Baldo, M. E. Thompson, S. R. Forrest, *J. Appl. Phys.* **2001**, *90*, 5048 – 5051; b) L. Xiao, S.-J. Su, Y. Agata, H. Lan, J. Kido, *Adv. Mater.* **2009**, *21*, 1271 – 1274.

[4] a) Z. Zhang, J. Xie, H. Wang, B. Shen, J. Zhang, J. Hao, J. Cao, Z. Wang, *Dyes Pigm.* **2016**, *125*, 299 – 308; b) Y. Feng, P. Li, X. Zhuang, K. Ye, T. Peng, Y. Liu, Y. Wang, *Chem. Commun.* **2015**, *51*, 12544 – 12547.

[5] a) S. Zhang, Q.-L. Xu, J.-C. Xia, Y.-M. Jing, Y.-X. Zheng, J.-L. Zuo, *J. Mater. Chem. C* **2015**, *3*, 11540 – 11547; b) K. S. Yook, J. Y. Lee, *J. Lumin.* **2015**, *161*, 271 – 274.

[6] a) S. Thiery, D. Tondelier, B. Geffroy, E. Jacques, M. Robin, R. Métivier, O. Jeannin, J. Rault-Berthelot, C. Poriel, *Org. Lett.* **2015**, *17*, 4682 – 4685; b) G. H. Kim, R. Lampade, M. J. Park, H. W. Bae, J. H. Kong, J. H. Kwon, J. H. Park, Y. W. Park, C. E. Song, *J. Phys. Chem. C* **2014**, *118*, 28757 – 28763; c) K. Thangaraju, J. Lee, J.-I. Lee, H. Y. Chu, Y.-H. Kim, S.-K. Kwon, *AIP Conf. Proc.* **2015**, *1667*, 060019 – 060011/060013; d) S. Hashimoto, T. Ikuta, K. Shiren, S. Nakatsuka, J. Ni, M. Nakamura, T. Hatakeyama, *Chem. Mater.* **2014**, *26*, 6265 – 6271; e) C. W. Lee, J. Y. Lee, *Chem. Commun.* **2013**, *49*, 6185 – 6187; f) J.-H. Jou, S. Sahoo, S. Kumar, H.-H. Yu, P.-H. Fang, M. Singh, G. Krucaite, D. Volyniuk, J. V. Grazulevicius, S. Grigalevicius, *J. Mater. Chem. C* **2015**, *3*, 12297 – 12307; g) Z. M. Hudson, Z. Wang, M. G. Helander, Z.-H. Lu, S. Wang, *Adv. Mater.* **2012**, *24*, 2922 – 2928; h) G. H. Kim, R. Lampande, J. H. Kong, J. M. Lee, J. H. Kwon, J. K. Lee, J. H. Park, *RSC Adv.* **2015**, *5*, 31282 – 31291.

[7] a) K. S. Yook, J. Y. Lee, *Adv. Mater.* **2012**, *24*, 3169 – 3190; b) M. Romain, S. Thiery, A. Shirinskaya, C. Declairieux, D. Tondelier, B. Geffroy, O. Jeannin, J. Rault-Berthelot, R. Métivier, C. Poriel, *Angew. Chem. Int. Ed.* **2015**, *54*, 1176 – 1180; *Angew. Chem.* **2015**, *127*, 1192 – 1196; c) M. Romain, D. Tondelier, B. Geffroy, O. Jeannin, E. Jacques, J. Rault-Berthelot, C. Poriel, *Chem. Eur. J.* **2015**, *21*, 9426 – 9439; d) H. Liu, Q. Bai, L. Yao, D. Hu, X. Tang, F. Shen, H. Zhang, Y. Gao, P. Lu, B. Yang, Y. Ma, *Adv. Funct. Mater.* **2014**, *24*, 5881 – 5888; e) M. Kim, S. K. Jeon, J. Y. Lee, *RSC Adv.* **2015**, *5*, 100378 – 100383; f) S. Thiery, D. Tondelier, C. Declairieux, B. Geffroy, O. Jeannin, R. Métivier, J. Rault-Berthelot, C. Poriel, *J. Phys. Chem. C* **2015**, *119*, 5790 – 5805; g) S. Thiery, C. Declairieux, D. Tondelier, G. Seo, B. Geffroy, O. Jeannin, R. Métivier, J. Rault-Berthelot, C. Poriel, *Tetrahedron* **2014**, *70*, 6337 – 6351; h) C. W. Lee, J. Y. Lee, *Chem. Mater.* **2014**, *26*, 1616 – 1621; i) S. Gong, Y.-L. Chang, K. Wu, R. White, Z.-H. Lu, D. Song, C. Yang, *Chem. Mater.* **2014**, *26*, 1463 – 1470; j) Y. P. Jeon, K. S. Kim, K. K. Lee, I. K. Moon, D. C. Choo, J. Y. Lee, T. W. Kim, *J. Mater. Chem. C* **2015**, *3*, 6192 – 6199; k) H. Liu, G. Cheng, D. Hu, F. Shen, Y. Lv, G. Sun, B. Yang, P. Lu, Y. Ma, *Adv. Funct. Mater.* **2012**, *22*, 2830 – 2836; l) C. Han, F. Zhao, Z. Zhang, L. Zhu, H. Xu, J. Li, D. Ma, P. Yan, *Chem. Mater.* **2013**, *25*, 4966 – 4976; m) C. W. Lee, J. Y. Lee, *Chem. Commun.* **2013**, *49*, 1446 – 1448; n) T.-L. Chiu, H.-J. Chen, Y.-H. Hsieh, J.-J. Huang, M.-k. Leung, *J. Phys. Chem. C* **2015**, *119*, 16846 – 16852; o) Y.-M. Xie, L.-S. Cui, F.-S. Zu, F. Igbari, M.-M. Xue, Z.-Q. Jiang, L.-S. Liao, *Org. Electron.* **2015**, *26*, 25 – 29.

[8] a) E. Baranoff, B. F. E. Curchod, *Dalton Trans.* **2015**, *44*, 8318 – 8329; b) C. Adachi, R. C. Kwong, P. Djurovich, V. Adamovich, M. A. Baldo, M. E. Thompson, S. R. Forrest, *Appl. Phys. Lett.* **2001**, *79*, 2082 – 2084.

[9] S.-J. Yeh, M.-F. Wu, C.-T. Chen, Y.-H. Song, Y. Chi, M.-H. Ho, S.-F. Hsu, C. H. Chen, *Adv. Mater.* **2005**, *17*, 285 – 289.

[10] S. H. Kim, J. Jang, S. J. Lee, J. Y. Lee, *Thin Solid Films* **2008**, *517*, 722 – 726.

[11] a) S. J. Lee, K.-M. Park, K. Yang, Y. Kang, *Inorg. Chem.* **2009**, *48*, 1030 – 1037; b) N. Jung, E. Lee, J. Kim, H. Park, K.-M. Park, Y. Kang, *Bull. Korean Chem. Soc.* **2012**, *33*, 183 – 188.

[12] F. Kessler, Y. Watanabe, H. Sasabe, H. Katagiri, M. K. Nazeeruddin, M. Grätzel, J. Kido, *J. Mater. Chem. C* **2013**, *1*, 1070 – 1075.

[13] a) S. Thiery, D. Tondelier, C. Declairieux, G. Seo, B. Geffroy, O. Jeannin, J. Rault-Berthelot, R. Métivier, C. Poriel, *J. Mater. Chem. C* **2014**, *2*, 4156 – 4166; b) L.-S. Cui, Y.-M. Xie, Y.-K. Wang, C. Zhong, Y.-L. Deng, X.-Y. Liu, Z.-Q. Jiang, L.-S. Liao, *Adv. Mater.* **2015**, *27*, 4213 – 4217.

[14] a) L. Ding, S.-C. Dong, Z.-Q. Jiang, H. Chen, L.-S. Liao, *Adv. Funct. Mater.* **2015**, *25*, 645 – 650; b) B. Pan, B. Wang, Y. Wang, P. Xu, L. Wang, J. Chen, D. Ma, *J. Mater. Chem. C* **2014**, *2*, 2466 – 2469; c) Y. Liu, L.-S. Cui, M.-F. Xu, X.-B. Shi, D.-Y. Zhou, Z.-K. Wang, Z.-Q. Jiang, L.-S. Liao, *J. Mater. Chem. C* **2014**, *2*, 2488 – 2495; d) F.-M. Hsu, L.-J. Chien, K.-T. Chen, Y.-Z. Li, S.-W. Liu, *Org. Electron.* **2014**, *15*, 3327 – 3332; e) S.-C. Dong, C.-H. Gao, X.-D. Yuan, L.-S. Cui, Z.-Q. Jiang, S.-T. Lee, L.-S. Liao, *Org. Electron.* **2013**, *14*, 902 – 908.

[15] It should be stressed that this design was originally introduced by Adachi et al. for thermally activated delayed fluorescence (TADF): K. Nasu, T. Nakagawa, H. Nomura, C.-J. Lin, C.-H. Cheng, M.-R. Tseng, T. Yasuda, C. Adachi, *Chem. Commun.* **2013**, *49*, 10385 – 10387.

[16] a) M. Romain, D. Tondelier, B. Geffroy, A. Shirinskaya, O. Jeannin, J. Rault-Berthelot, C. Poriel, *Chem. Commun.* **2015**, *51*, 1313 – 1315; b) M. Romain, D. Tondelier, O. Jeannin, B. Geffroy, J. Rault-Berthelot, C. Poriel, *J. Mater. Chem. C* **2015**, *3*, 9701 – 9714.

[17] a) S. O. Jeon, J. Y. Lee, *Tetrahedron* **2010**, *66*, 7295 – 7301; b) M. S. Park, J. Y. Lee, *Thin Solid Films* **2013**, *548*, 603 – 607; c) J.-A. Seo, M.-S. Gong, J. Y. Lee, *Org. Electron.* **2014**, *15*, 1843 – 1848; d) J.-A. Seo, M. S. Gong, J. Y. Lee, *Org. Electron.* **2014**, *15*, 3773 – 3779; e) Y.-X. Zhang, L. Ding, X.-Y. Liu, Z.-Q. Jiang, H. Chen, S.-J. Ji, L.-S. Liao, *Org. Electron.* **2015**, *20*, 112 – 118.

[18] S. C. To, F. Y. Kwong, *Chem. Commun.* **2011**, *47*, 5079 – 5081.

[19] M. J. Plater, S. Kemp, E. Lattmann, *J. Chem. Soc. Perkin Trans. 1* **2000**, 971 – 979.

[20] M.-H. Tsai, Y.-H. Hong, C.-H. Chang, H.-C. Su, C.-C. Wu, A. Matoliukstyte, J. Simokaitiene, S. Grigalevicius, J. V. Grazulevicius, C.-P. Hsu, *Adv. Mater.* **2007**, *19*, 862 – 866.

[21] a) J. Rault-Berthelot, J. Simonet, *J. Electroanal. Chem.* **1985**, *182*, 187 – 192; b) J. Rault-Berthelot, M.-M. Granger, L. Mattiello, *Synth. Met.* **1998**, *97*, 211 – 215; c) J. Rault-Berthelot, L. Angely, J. Delaunay, J. Simonet, *New J. Chem.* **1987**, *11*, 487 – 494; d) J. Rault-Berthelot, M.-A. Orliac, J. Simonet, *Electrochim. Acta* **1988**, *33*, 811 – 823.

[22] C. Poriel, J.-J. Liang, J. Rault-Berthelot, F. Barrière, N. Cocherel, A. M. Z. Slawin, D. Horhant, M. Virboul, G. Alcaraz, N. Audebrand, L. Vignau, N. Huby, G. Wantz, L. Hirsch, *Chem. Eur. J.* **2007**, *13*, 10055 – 10069.

[23] S.-C. Dong, Y. Liu, Q. Li, L.-S. Cui, H. Chen, Z.-Q. Jiang, L.-S. Liao, *J. Mater. Chem. C* **2013**, *1*, 6575 – 6584.

[24] Y.-X. Zhang, L. Zhang, L.-S. Cui, C.-H. Gao, H. Chen, Q. Li, Z.-Q. Jiang, L.-S. Liao, *Org. Lett.* **2014**, *16*, 3748 – 3751.

[25] M. Hong, K. Zhang, Y.-Z. Li, J. Zhu, *Polyhedron* **2009**, *28*, 445 – 452.

[26] K. Brunner, A. van Dijken, H. Börner, J. J. A. M. Bastiaansen, N. M. M. Kiggen, B. M. W. Langeveld, *J. Am. Chem. Soc.* **2004**, *126*, 12619.

[27] a) H. Ye, D. Chen, M. Liu, S.-J. Su, Y.-F. Wang, C.-C. Lo, A. Lien, J. Kido, *Adv. Funct. Mater.* **2014**, *24*, 3268 – 3275; b) T. Earmme, S. A. Jenekhe, *J. Mater. Chem.* **2012**, *22*, 4660 – 4668; c) J.-K. Bin, N.-S. Cho, J.-I. Hong, *Adv. Mater.* **2012**, *24*, 2911 – 2915.

[28] J. G. Jang, H. J. Ji, H. S. Kim, J. C. Jeong, *Curr. Appl. Phys.* **2011**, *11*, S251 – S254.

[29] CCDC CCDC-1436575 for **SIA-F** and -1436574 for **SIA-TXO$_2$** contain the supplementary crystallographic data for this paper. These data are provided free of charge by The Cambridge Crystallographic Data Centre.

Received: February 11, 2016
Published online on ■■ ▮▮, 0000

FULL PAPER

Phosphorescent OLEDs: Detailed structure–property relationship study of a series of efficient host materials based on the indoloacridine core is reported. These materials have been incorporated in green and sky-blue PhOLEDs with high performance displaying the potential of the indoloacridine fragment.

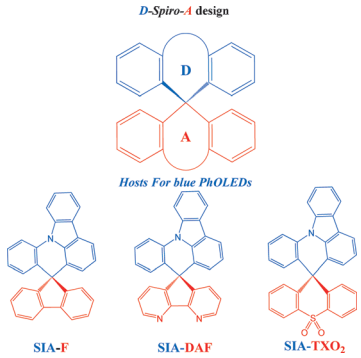

Organic Semiconductors

S. Thiery, D. Tondelier, B. Geffroy, O. Jeannin, J. Rault-Berthelot, C. Poriel**

■■ – ■■

Modulation of the Physicochemical Properties of Donor–Spiro–Acceptor Derivatives through Donor Unit Planarisation: Phenylacridine versus Indoloacridine. New Hosts for Green and Blue Phosphorescent Organic Light-Emitting Diodes (PhOLEDs)